

1 **REVISION 2**

2 **Crystal structure of Ag-exchanged levyne intergrown with erionite: single crystal X-ray**
3 **diffraction and molecular dynamics simulations**

4 Georgia Cametti^{1*}, Sergey V. Churakov^{1,2}

5 ¹Institute of Geological Sciences, Mineralogical Crystallography, Baltzerstrasse 1+3, 3012 Bern,
6 Switzerland

7 ²Paul Scherrer Institut, Forschungstrasse 111, 5232 Villingen PSI, Switzerland

8 *Corresponding author: georgia.cametti@krist.unibe.ch

9 **ABSTRACT**

10 The modification of natural zeolites *via* ion exchange is an efficient technique used to improve
11 their performances and tune their properties for specific applications. In this study, a natural
12 levyne-Ca intergrown with erionite was fully exchanged by Ag⁺ and its structure (with idealized
13 chemical composition Ag₆(Si,Al)₁₈O₃₆·18H₂O) was investigated by combining a theoretical and
14 experimental approach. Single crystal X-ray diffraction data demonstrated that Ag-levyne
15 maintained the *R-3m* space group, characteristic of the natural levyne. Ag ions distribute over
16 partially occupied sites along the three-fold axis and, differently from the pristine material, at the
17 wall of the 8-membered ring window of the *lev* cavity. The lack of approximately 30% of Ag
18 ions that could not be located by the structural refinement is ascribed to the strong disorder of the
19 extraframework occupants. The structural results obtained by molecular dynamics simulations are
20 in overall agreement with the experimental data and showed that, on average, Ag⁺ is surrounded
21 by approximately 2 H₂O and 1 framework oxygen at distances between 2.43 and 2.6 Å.
22 Molecular dynamics trajectories indicate that the occurrence of silver inside the D6R cage

23 depends on the water content: silver occupancy of D6R cages is estimated to be 83%, 30%, and
24 0% when the structure contains 3, 2.5, and 2 H₂O per Ag ion, respectively.

25 The cation-exchange process, as demonstrated by SEM-EDS analyses affects the intergrown
26 erionite as well. A structural characterization of the Ag-erionite phase (with dimension less than
27 100 μm) was possible by means of a CuKα micro-focus source: structure solution pointed to
28 *P6₃/mmc* space group, indicating no change with respect to natural erionite. In agreement with
29 previous studies, K ions in the cancrinite cage could not be exchanged, whereas Ag⁺ is found in
30 the *eri* cavity.

31 **Keywords:** Zeolites, Ag-levyne, LEV, Ag-erionite, X-ray Diffraction, Molecular dynamics

32 INTRODUCTION

33 The mineral series levyne, comprising levyne-Ca and levyne-Na, belongs to the zeolites group.
34 The crystal structure of these minerals is described by a three-dimensional aluminosilicate
35 tetrahedral framework in which charge compensating alkali and/or alkaline earth cations and H₂O
36 occupy the structural voids. Due to their microporous structure, zeolite minerals show interesting
37 properties such as cation exchange, adsorption, reversible hydration/dehydration and the capacity
38 of acting as molecular sieves (Bish and Ming 2001). For this reason, they are successfully applied
39 for a broad range of applications, and in particular in environmental remediation processes
40 (treatment of radioactive wastewater and remediation of contaminated sites (Colella 1999; Babel
41 et al. 2003; Borai et al. 2009; Misaelides 2011; Wang et al. 2010). Compared to their synthetic
42 counterpart, natural zeolites typically show greater thermal stability and better resistance to acid
43 environments (Ackley et al. 2003). Rich opportunities for technological applications, abundance
44 in nature and low mining costs, motivate research on structural and chemical properties of natural
45 zeolites in various scientific disciplines.

46 **LEV**-type zeolites are of interest because, despite their small pore openings, they show large
47 micropore volume ($0.3 \text{ cm}^3/\text{g}$) (Yamamoto et al. 2010). Thus, several phases with **LEV** topology
48 have also been synthesized (Flanigen et al. 1986; Lock et al. 1984; Zhu et al. 1997) and Ca-LEV
49 was suggested as potential hydrogen-storage medium (Liang et al. 2012).

50 The natural occurring levyne belongs to the so-called ABC-6 family of natural zeolites (Gottardi
51 and Galli, 1985). The **LEV** framework type of levyne is characterized by a sequence of single
52 six-membered rings (6mR) and double six-membered rings (D6R) of tetrahedra stacked along the
53 c axis following the AABCCABBCAA sequence. This sequence originates columns along [001]
54 of cavities [$4^9 6^5 8^3$] (*lev* cavity), which alternates with double six-ring [$4^6 6^2$] polyhedra. Two
55 dimensionally interconnected channels confined by eight-membered rings run perpendicular to
56 [001]. The crystal structure at room temperature is described in *R-3m* space group (Merlino et al.
57 1975; Sacerdoti 1996). Natural crystals of levyne are often twinned by 180° rotation along the c
58 axis simulating *P6/mmm* symmetry (Sacerdoti, 1996). Moreover, intergrowths with
59 erionite/offretite, two other zeolites pertaining to the ABC-6 family, have been frequently
60 reported in natural occurring levyne (Shimazu and Mizota 1972; Bennett and Grose 1978; Wise
61 and Tschernich 1976; Passaglia et al. 1974).

62 The microporous properties of natural zeolites are controlled by the extraframework (EF) cations
63 content. The modification of their crystal-structure *via* cation exchange has been proven to
64 improve their performances over a wide range of applications (Kasture et al. 1998; Ackley et al.
65 2003; Kanazawa, 2004; Zukal et al. 2010; Amooghin et al. 2016; Ma et al. 2018; Abreu et al.
66 2019). In particular, Ag-exchanged zeolites show increased sorption and photocatalytic capacity
67 (Hutson et al. 2000; Coutino-Gonzales et al. 2015) and antibacterial efficacy (Milenkovic et al.
68 2017; Ferreira et al. 2012). To predict the zeolites behavior in terms of stability and microporous

69 properties two factors are particularly important: i) the position of the EF cations in relation to the
70 aluminosilicate framework, and ii) the modification of the framework itself as a consequence of
71 the EF cations substitution.

72 In this study, we investigate the crystal structure of Ag-levyne produced by cation exchange of a
73 natural levyne-Ca. In order to determine the EF cation arrangement in the zeolitic channels and to
74 have a better insight into the local environment of silver atoms and global structural disorder, we
75 combined an experimental and theoretical approach. The average structural parameters were
76 determined by means of single crystal X-ray diffraction and compared with that obtained by
77 molecular dynamics simulations. Moreover, a detailed structural characterization of the erionite
78 intergrowths was also undertaken.

79 MATERIALS AND METHODS

80 The sample used as starting material was a natural levyne with chemical composition
81 $\text{Ca}_{2.53}\text{Na}_{0.72}\text{K}_{0.23}(\text{Al}_{6.26}\text{Si}_{11.8}\text{O}_{36}) \cdot 17.58\text{H}_2\text{O}$ from Beech Creek, Oregon, USA. The crystals were
82 selected from the same specimen (sample number A7827 of Natural History Museum of Bern)
83 used by Cametti (2018).

84 The exchange experiments were performed following two steps: at first, levyne crystals with
85 dimensions ranging from 0.08 and 0.3 mm were treated for four weeks with 1M NaCl solution at
86 $100(2)^\circ\text{C}$ in a Teflon autoclave. The solution was renewed every three days. Afterwards, the Na-
87 exchanged crystals were equilibrated with a 2M AgNO_3 solution ($\text{pH} = 5-6$) at $100(2)^\circ\text{C}$ for 5
88 weeks. For this second exchange-step, the crystals were also located in a Teflon autoclave and
89 darkness conditions were maintained during the whole experiment. The AgNO_3 solution was
90 periodically renewed every 3 days. The crystals were subsequently removed from the autoclave,
91 washed with deionized water and analyzed by energy-dispersive spectrometry (EDS) using a

92 ZEISS EVO50 scanning electron microscope (SEM) to ensure the completeness of the exchange
93 process. Operating conditions were 20kV accelerating voltage, 10 mm working distance, 30 s
94 acquisition time. An attempt to analyze the same samples with electron microprobe was not
95 successful due to the small crystal size. Final chemical composition was calculated on the basis
96 of 36 O after renormalization of the chemical analyses hypothesizing a water content of 18% wt.

97 **Single crystal X-ray diffraction (SCXRD)**

98 Diffraction data were collected on a Bruker APEX II diffractometer equipped with a MoK α
99 source ($\lambda = 0.71073$) and a CCD detector. A single crystal of Ag-levyne with dimension 0.180 x
100 0.150 x 0.100 mm was glued on the tip of a glass fiber and mounted on a goniometer head.

101 The unit cell determination indicated a rhombohedral Bravais-lattice. An inspection of the
102 reciprocal lattice pointed out the presence of an additional set of reflections (approximately 6-7%
103 of the total ones) that could be indexed with the same rhombohedral unit-cell rotated by 180°
104 with respect to the *c*-axis. The data were integrated and corrected for absorption by using the
105 Apex 3v.2018.7-2 software package (Bruker AXS 2017).

106 The structure was solved in space group *R-3m* by direct methods using Shelxtl-2008 (Sheldrick
107 2008). Structural refinement was carried out by SHELXL-2014 (Sheldrick 2015) by using neutral
108 atomic scattering factors. Starting coordinates and atomic labels of framework atoms were those
109 reported in Sacerdoti (1996) whereas the EF cations and H₂O molecules were located by
110 difference Fourier maps. The obverse-reverse twinning [-100 0-10 001] was refined with
111 fractional volume contribution of 0.058(4).

112 Erionite and offretite intergrowths have been frequently reported for levyne specimen from the
113 same locality (Bennett and Grose, 1978; Passaglia et al. 1998; Cametti 2018). SEM-BSD pictures
114 of our sample showed the occurrence of another fibrous-mineral phase intergrown between
115 levyne crystals (Fig. 1). To find out whether the intergrown mineral was erionite or offretite and

116 to determine how this phase was affected by the exchange experiments, single fragments of
117 secondary phase were extracted to perform subsequent structural analyses. Fragments of Ag-
118 exchange levynite were at first carefully inspected under a binocular microscope and disintegrated
119 into smaller pieces with dimensions less than 100 μm . To find the erionite/offretite crystals,
120 several fragments were preliminary checked by single-crystal X-ray diffraction, in order to
121 extrapolate the unit-cell parameters. Finally, a crystal with dimension of approximately $0.05 \times$
122 0.03×0.015 mm was identified as erionite.

123 A single crystal of erionite-Ag was glued on the tip of a glass fiber and mounted on a goniometer
124 head. Diffraction data were collected on a Synergy-S Rigaku dual micro-focused source
125 diffractometer equipped with a HyPix detector. The $\text{CuK}\alpha$ ($\lambda = 1.54184$) radiation was chosen for
126 data collection due to the small dimensions of the crystal under investigation. An attempt to
127 measure the same sample with $\text{AgK}\alpha$, available on the same machine, or with $\text{MoK}\alpha$ used for the
128 Ag-levynite X-ray data collection, was not successful because of the low diffracting power of such
129 a small crystal fragment. Diffraction data were integrated and corrected for absorption by using
130 CrysAlisPro 171.40.29a (Rigaku Oxford Diffraction, 2018). Erionite crystal structure was solved
131 by direct methods in space group $P6_3/mmc$.

132 Crystal data, collection and refined parameters are reported in Table S1. Crystallographic
133 information file (Cif) of the refined structures has been deposited as supplementary material. The
134 drawings of the crystal structures were produced by VESTA (Momma and Izumi, 2011).

135

136 **Molecular dynamics (MD) simulations**

137 Molecular dynamics simulations were performed using the CP2K simulation package
138 (www.cp2k.org). The equations of motion were integrated using a 0.5 fs time step. The
139 interatomic forces were calculated based on Density Functional Theory (DFT) using the Gaussian

140 and plane waves methods (VandeVondele et al. 2005a). The electron exchange and correlations
141 were described by Perdew-Burke-Ernzerhof functional (PBE) (Perdew et al. 1996). Dispersion
142 interaction was taken into account using the DFT+D2 method (Grimme et al. 2006). The
143 calculations were carried out in NPT ensemble (constant pressure and temperature using a fully
144 flexible cell). Indeed, although atomistic simulations with fixed cell parameters can provide a
145 satisfactory atomistic description of the extraframework content (Gatta et al. 2018), NPT
146 ensemble was chosen in this study to take into account the strong disorder of the EF content and
147 improve the convergence toward the stable configuration.

148 The simulations temperature of MD was set to 77°C to prevent the glassy behavior of PBE-H₂O
149 (VandeVondele et al. 2005b). The use of slightly elevated temperature makes sure ergodic
150 dynamic of ions and water in the channels. The experimental measurements suggest that the
151 space group symmetry does not change with in the given temperature range. The Kohn-Sham
152 orbitals were expanded using a linear combination of atom centered Gaussian-type orbital
153 functions. A “short-range” double- valence polarized basis set MOLOPT was used for each
154 atomic kind (VandeVondele and Hutter, 2007). Similar setup was successfully used in our
155 previous simulations of zeolites (Cametti et al. 2019a; Cametti et al. 2019b).

156 The simulation supercell ($2 \times 1 \times 1$) contained 684 atoms (36 Ag, 36 Al, 72 O, 216 O, 108 H₂O).
157 The starting coordinates of the framework atoms were those of levyne-Ca (Cametti 2018). Silicon
158 was randomly substituted by aluminum according to the bulk chemical composition following the
159 Loewenstein’s rule (Loewenstein, 1954). The Ag atoms were initially placed along the three-fold
160 axis parallel to [001] in the middle of each [4⁹6⁵8³] cavity. The number of H₂O was set according
161 to the idealized chemical composition of levyne that is 3.0 H₂O per EF cation (Passaglia and
162 Sheppard, 2001). The structural data were collected from a 25 ps-long MD trajectory followed by

163 at least 6 ps pre-equilibration. Moreover, two additional structural models with 2.5 and 2 H₂O per
164 Ag atom, respectively, were tested.

165

166

RESULTS

167 The EDS-SEM analyses of the Ag-exchanged levyne showed that Na⁺ was completely replaced
168 by Ag⁺. The detected amount of potassium was related to the occurrence of erionite intergrowths
169 as confirmed by SEM pictures (Fig. 1). Within the same single crystal, two main domains can be
170 recognized: one with a fibrous-like morphology, which mainly contains K and Ag as EF cations
171 and, the other that is K-free. This kind of intergrowths, i.e. erionite on the {0001} faces of levyne
172 lamellae is frequent and was observed in samples from different localities (Passaglia et al. 1974;
173 Bennet and Grose, 1978; Wise and Tschernich, 1976; Gottardi and Galli, 1985). Final chemical
174 composition for Ag-levyne and -erionite are Ag_{6.1}Al_{6.3}Si_{11.8}O₃₆·18.0H₂O and
175 Ag_{8.9}K_{1.7}Al_{10.1}Si_{22.5}O₇₂·30H₂O, respectively.

176 Crystal structure of Ag-levyne

177 The Ag-levyne structure at RT preserves the space group *R-3m* characteristic of the natural
178 levyne-Ca. The aluminosilicate framework did not show significant changes because of Ag⁺
179 uptake. The unit cell parameters were comparable with those of the pristine material (Cametti,
180 2018). The dimension (6.48 × 7.39 Å) of the apertures of the 8-membered ring channels along
181 [100] was similar to that of levyne-Ca (6.44 × 7.42 Å).

182 The structural refinement of the XRD data indicated that Ag ions are strongly disordered within
183 the zeolitic pores. Four main EF Ag sites (Ag1, Ag2, Ag3, and Ag4) were located plus additional
184 low-occupied sites (Ag1A, Ag2A, Ag2B, Ag4A,...Ag4E) (occupancy less than 0.15) close to the
185 main ones (Fig. 2, Table S2). The Ag1 site is the most populated, with occ. = 0.429(19). In Ag-

186 levyne, the Ag sites (Ag1, Ag2, and Ag3) are distributed along the 3- fold axis and, different to
187 the EF cations in natural levyne-Ca, at the wall of the eight-membered ring window of the *lev*
188 cage (Ag4) (Fig. 2). Ag ions at this position are extremely disordered and a simultaneous
189 presence of Ag and H₂O cannot be excluded.

190 In natural levyne-Ca (Cametti, 2018), EF cations and H₂O are found at five sites: (C1, C2, C3,
191 C4, C5) and (W1, W2, W3, W4, and W5), respectively. In Ag-levyne:

- 192 • Ag1 site corresponds to C1 that in levyne-Ca is almost fully occupied by Ca;
- 193 • Ag3 site corresponds to C2, which in levyne-Ca is 13% occupied by Ca;
- 194 • Ag2, Ag2A, and Ag2B correspond to C3, C4, and C5 respectively; these positions in
195 natural levyne-Ca, are partially occupied by Na, K, and Ca respectively (Cametti, 2018).
- 196 • The positions of Ag4 sites (Ag4A, Ag4B, Ag4C, Ag4D, and Ag4E) are comparable to
197 those of H₂O at W2, W4, and W5 in levyne-Ca;
- 198 • W1 and W3 positions are identical in levyne-Ca and Ag-levyne.

199 Relevant bond distances of Ag-levyne structure are reported in Table 1. Ag1 site is coordinated
200 by three H₂O at W1 (2.372(8) Å) and three framework-oxygen atoms at O2 (2.470(5) Å),
201 forming a fairly regular octahedron. Ag2 site bonds to six framework-oxygen atoms at O5
202 (2.591(5) Å), which constitute the aperture of the six-membered ring window of the *lev* cavity.
203 Bond distances between 2.24 and 2.6 Å are found for Ag4A, Ag4B, Ag4C, Ag4D, and Ag4E. On
204 average, the sites at these positions bond to three oxygen atoms of the 8-membered ring aperture
205 (two at O1 and one at O3) and two H₂O at W3.

206 The total number of Ag ions per formula unit obtained by the structural refinement was lower
207 compared to that estimated by the chemical analyses. On the basis of 36 oxygen, the total
208 number of positive charges required to balance the negative charge of the aluminosilicate

209 framework is 6. However, if all the EF sites are refined with Ag scattering factor, the refined Ag⁺
210 apfu is only 4, pointing out that approximately 30% of the EF silver could not be located by
211 XRD.

212 **Molecular dynamics**

213 The unit lattice constants obtained by MD simulations are close to those obtained by XRD, with a
214 deviation of less than 1% for all parameters and 1.75% for the length of the c-axis (Table 2).

215 Fig. 3 reports a snapshot of the structure obtained after 20 ps calculation. Ag atoms are found
216 mainly along the three-fold axis and part of them are displaced toward the 8-membered ring
217 window of the *lev* cavity. The radial distribution function (RDF) and running coordination
218 number (CN) of the Ag-O (O oxygen of the framework) and Ag-O_w (O_w oxygen of the H₂O) are
219 reported in Fig. 4. The RDF of the Ag-O_w distances show a clear peak at 2.43 Å, whereas the
220 curve corresponding to Ag-O indicates a broadened distribution of distances with a maximum at
221 ca. 2.5 Å. On average, each Ag is surrounded by approximately 2 H₂O and 1 framework oxygen
222 at distances between 2.43 and 2.60 Å.

223 The Ag ions in the *lev* cavity are found at the top and bottom of the cavity, close to the aperture
224 of the six-membered rings (Fig. 5a). These atoms are coordinated by three-framework oxygens
225 and by three H₂O, which occupy the central part of the cage. Additional Ag ions, located at the 8-
226 membered ring windows, bond to two framework oxygen atoms and to two or three H₂O (Fig.
227 5a). Such Ag distribution in the *lev* cavity agrees with that observed by the structural refinement
228 (Fig. 5b) where Ag ions disordered at Ag₄ sites are located on the wall of the aperture of the 8-
229 membered ring. Additional disordered Ag atoms at Ag₂ sites are distributed at the bottom of the
230 cage.

231 In the simulations setup with 3 H₂O per Ag atom, an additional Ag ion is found at (0,0,0), in the
232 middle of approximately 83% of the double six-membered rings (D6R) cage (Fig. 3). In contrast,
233 in the structural refinement, no residual electron density was found at this position and an attempt
234 to insert an additional site at (0,0,0) was not successful.

235 The hydrogen bond-net of the structure with 3 H₂O mainly involves oxygen of the water
236 molecules whereas no significant interactions between H and framework oxygens was observed
237 (each O has approximately only 0.2 H atoms within 2.0 Å Fig. S1). The RDF and CN of Ow···H
238 contacts shows that, on average, 0.5 H are found at distance of 1.70 Å from Ow, indicating a
239 medium-strong character of such interactions (Fig. S1). As expected, the number of the Ow···H
240 contacts decreases and becomes less significant if the modelled structures with 2 and 2.5 H₂O per
241 Ag ion are considered (Fig. S2). Detailed analysis of the Ow-H RDF shows that in agreement
242 with expected more acidic properties of the H₂O coordinating the Ag-ion, proton donation events
243 take place between water in Ag-coordination shell and interstitial water (Albuquerque and
244 Calzaferri, 2007; Fois and Tabacchi, 2019).

245 **Crystal structure of intergrown Ag-erionite**

246 The structural parameters of Ag-exchanged erionite and relevant bond distances are reported in
247 Table S3 and Table 3, respectively. The *P*6₃/*mmc* characteristic of the natural erionite (Alberti et
248 al. 1997) is preserved after the uptake of Ag ions. The unit-cell (*a* = 13.29919(19), *c* =
249 15.19312(19) Å, *V* = 2327.17(7) Å³) is slightly smaller compare to that of an erionite sample
250 from the same locality (*a* = 13.345(1), *c* = 15.124(3) Å, *V* = 2332.6(5) Å³) reported by Passaglia
251 et al. (1998). According to the structural refinement, K occupies the middle of the cancrinite
252 cage, where it is slightly displaced along *z* direction as demonstrated by the occurrence of an
253 additional site K1A (Occ. = 0.030(16)) at 0.8(3) Å from K1 (Occ. = 0.98(4)) (Fig. 6). This finding

254 is in agreement with Sherry (1979) who reported that potassium in the cancrinite cavities cannot
255 be replaced via ion exchange in aqueous solution because of the small opening of the 6-
256 membered ring window, which hampers the passage of the K ions.

257 Ag ions are distributed in the *eri* cavity, at disordered sites with partial occupancies (Fig. 6).

258 Three main positions can be recognized:

259 - C1, the most occupied site (Occ. = 0.679(14)) is located in the erionite cavity close to the
260 6-membered ring aperture of the cancrinite cage; it forms two bonds with framework
261 oxygen at O6 (2.500(6) Å) and two longer connections (2.986(5) Å) with those at O4. A
262 very low occupied site C1A close to C1 indicates, also in this case, a displacement from
263 the mirror plane perpendicular to [001].

264 - C2, disordered at three different subsites (C2, C2A, C2B, with total Occ. = 0.53)
265 distributes at the bottom and top of the erionite cavity, in the aperture center of the 6-
266 membered rings. Ag ions at this position form bonds with framework oxygen O5 of the
267 six-membered ring and with H₂O at W5 site, which is located along the three-fold axis.

268 - C3, C3A, and C3B (total Occ. = 0.21) are located in the middle of the *eri* cavity and bond
269 only to H₂O at W5A and W4A.

270 All water molecules, but those at W5 and W5A, are distributed over five sites at the wall of the
271 *eri* cavity in correspondence of the 8-membered ring window (Table S3, Fig. 6).

272 The total number of positive charges obtained by the structural refinement (11.3⁺) is in
273 reasonable agreement with that estimated by the chemical analysis (12.3⁺).

274

275

DISCUSSION

276 The analysis of the erionite intergrowths demonstrated that all EF cations in the *eri* cavity could
277 be exchanged with Ag⁺ and, differently from Ag-levyne, all Ag ions in the unit cell could be

278 located by the structural refinement. The lack of ca. 30% of Ag^+ in Ag-levyne structure can be
279 explained by: (i) migration of part of silver toward the external surface or (ii) strong disorder of
280 the remaining Ag^+ in the structural voids, which prevents its exact location.

281 Since positional disorder of EF sites was observed also in Ag-erionite, but all Ag could be
282 located, we decided to collect additional XRD data on Ag-levyne by using the more brilliant Cu
283 micro-focused source employed to investigate Ag-erionite. Other two fragments of Ag-levyne
284 were selected and data were collected on the same instrument used for Ag-erionite. As an
285 example, data-collection parameters and results obtained for the first fragment are reported in
286 Table S4 and S5. Structural refinements did not show any significant change in terms of EF
287 cation positions but, in both cases, the refined chemical composition indicated an Ag content
288 higher than 5 apfu. Such a value can be reasonably accepted, if the errors on refined values of
289 both occupancies and thermal parameters are taken into account (Table S5). Thus, the disorder
290 hypothesis (ii) seems the most reasonable. Such hypothesis is also supported by similar findings
291 in hydrated fully-exchange Ag-chabazite and Ag-heulandite (Nevenka et al. 1981; Calligaris et
292 al. 1983). In both cases, the authors could not locate by XRD methods all Ag ions revealed by the
293 chemical analyses. In Ag-exchanged heulandite, only 56 % of exchanged Ag^+ were detected by
294 X-ray (Nevenka et al., 1981). Similarly, in Ag-chabazite only 61% Ag^+ could be placed by the
295 structural refinement (Calligaris et al. 1983). The interpretation given by the authors was that
296 remaining Ag ions “spread out in the channels of the zeolite ... giving no detectable contribution
297 to the diffraction pattern” (Nevenka et al. 1981).

298
299 According to our findings, the distribution of Ag^+ in the two intergrown phases slightly differs. In
300 erionite, the disorder that affects the Ag ions is less pronounced; with the exceptions of C1A and
301 C3A, and C3B sites, the occupancies of all EF sites is higher than 0.15, and most part of Ag is

302 found at C1 site (Occ. = 0.679(14)). In Ag-levyne, apart from Ag1 (Occ. = 0.429(19)), ions are
303 distributed at sites with occupancies less than 0.15. In particular, silver ions at the wall of the *lev*
304 cavity are significantly disordered and affected by high displacement parameters that strongly
305 influence the final values of the refined occupancies.

306
307 Overall, the exchange of the original EF cations with Ag⁺ in the levyne structure does not induce
308 significant structural modifications of the framework. The Ag⁺ ions distribute at different
309 crystallographic sites compared to levyne-Ca and to levyne-Na. In particular, the sites at Ag4-
310 Ag4E sites are located at the aperture of the 8-membered rings of the *lev* cavity where in natural
311 levyne H₂O molecules are found. Such distribution was confirmed by the MD simulations, which
312 indicated a displacement of the EF cations away from the 3-fold axis. MD trajectories also
313 pointed out the occurrence of a silver ion located inside the D6R cage. However, according to
314 XRD results, no residual electron density was found at this position.

315 To explain this mismatch, we have to keep in mind that in real exchange experiments, not only
316 the availability but also the accessibility of the EF sites must be considered; the latter is related to
317 the kinetic behavior of the ion-exchange system and thus to the diffusion coefficients of that
318 specific ion within the pores (Inglezakis et al. 2004). The diffusion and the ability of an ion to
319 access a specific site may depend on its hydration shell. From the structural refinement, we could
320 not unambiguously determine the exact water content, due to the strong disorder of the EF
321 occupants. MD simulations with 3 H₂O per Ag ion, represent an idealized chemical composition
322 of levyne-(Ca_{0.5},Na)₆ (Passaglia and Sheppard, 2001). However, in Ag-levyne, the number of EF
323 cations is 1.5 greater than in levyne-Ca (1 Na plus 2.5 Ca apfu). A possible reason of the
324 presence of Ag⁺ inside the D6R cage could be the overestimation of the number of structural

325 H₂O; less room for Ag ions in the *lev* cavity, would force them to enter inside the D6R cage. To
326 test the effect of H₂O amount on the Ag distribution in **LEV** framework type, additional
327 molecular dynamics simulations (12 ps long trajectories) of Ag-levyne structure with different
328 water content were performed. At first, we hypothesized 2.5 H₂O (instead of 3) per Ag ion that is
329 15 H₂O pfu. With such configuration, only 30% of the D6R cage is occupied by a Ag ion. When
330 removing an additional 0.5 H₂O, i.e. modelling a structure with only 2 H₂O per Ag ion (12 H₂O
331 pfu) no EF cations are found inside the cage at (0,0,0) (Fig. 7). In both cases, displacement of part
332 of Ag ions from the three-fold axis toward the 8-membered ring window was observed.

333 Based on these results, the structure containing 2 H₂O per Ag ion represents the best agreement
334 between experimental (XRD) and calculated (MD) Ag-levyne. It should be kept in mind that the
335 amount of structural (and absorbed) water in a zeolitic material is strongly influenced by the
336 environmental conditions the sample is exposed to (i.e. relative humidity, temperature). It is
337 worth to mention, that in one of the data set collected as test purpose (by using the Cu micro-
338 focus source) on a fragment of Ag-levyne, a tiny peak at (0,0,0) appeared in the difference
339 Fourier maps. Nevertheless, an attempt to insert it in the structural refinement did not lead to
340 satisfactory results, being the refined value as big as the computed error. Interestingly, the
341 occurrence of a cation at this position, i.e. (0,0,0), was found in the dehydrated form of levyne-Ca
342 (Arletti et al. 2013, Cametti, 2018).

343

344

IMPLICATIONS

345 Currently, natural zeolites are effectively applied for waste-water treatment and removal of
346 contaminants. On the other hand, their use in other important fields such as catalysis or gas
347 separation processes is still limited. In the last decades, much effort has been made to improve

348 the catalytic and separation potential. The functionalization and modification of the natural
349 zeolites by thermal treatment or ion-exchange has been one of the most used and successful
350 technique (Zukal et al. 2010; Ma et al. 2017; Abreu et al. 2019; Velazquez-Pena et al. 2019). The
351 specific case of Ag-modified zeolites is particularly interesting, because silver is known to
352 strongly influence the adsorption characteristics of aluminosilicate zeolites (Hutson 2000). For
353 example, modified Ag-ferrierite and Ag-mordenite are applied in air purification processes
354 (Ar/O₂ enrichment or exhaust gas cleanup) (Knaebel and Kandybin, 1993; Ogawa et al. 2001). In
355 addition, Ag-exchanged zeolites have attracted great attention due their remarkable luminescent
356 and photocatalytic properties (De Cremer et al. 2009; Countino-Gonzales et al. 2015; Aghakhani
357 et al. 2018). In this context, particular attention must be paid not only to the framework topology
358 and to the size of the micro pores but also, and especially, to the cation positions in the structural
359 voids (Seifert et al. 2000; Aghakhani et al. 2018; Fron et al. 2019). Previous researches on
360 transition-metals modified zeolites have shown that even if the structure experiences little
361 modifications of the framework at RT, the new EF cations have a significant influence on the
362 dehydration path (i.e. phase transformations) and thermal stability of the new-produced zeolite.
363 With this respect, a high temperature structural study is in progress to check whether Ag-levyne
364 will undergo, upon heating, different structural changes compare to levyne-Ca.

365
366 **Acknowledgement**

367 We are thankful to Dr. Beda Hoffman of Natural History Museum of Bern who provided the
368 levyne sample, Dr. Mariko Nagashima for her help with EMPA analyses, and to Thomas
369 Armbruster for reading the manuscript. We acknowledge access to the Swiss National
370 Supercomputing Center (CSCS) and UBELIX HPC cluster at the University of Bern. The Swiss
371 National Science Foundation (SNF) is acknowledged for the Ambizione grant n. PZ00P2 173997

372 awarded to G. C. and for the R'Equip grant n. 206021_177033 awarded to P. Macchi. Gloria
373 Tabacchi and an anonymous reviewer are thanked for their very constructive comments.

374

375 REFERENCES

376

377 Abreu, N. J., Valdés, H., Zaror, A. C., Azzolina-Jury, F., Meléndrez, M. F. (2019) Ethylene
378 adsorption onto natural and transition metal modified Chilean zeolite: An *operando* DRIFTS
379 approach. *Microporous and Mesoporous Materials*, 274, 134-148.

380 Ackley, M. W., Rege, S. U., Saxena, H. (2003) Application of natural zeolites in the purification and
381 separation of gases. *Microporous and Mesoporous Materials*, 61, 25-42.

382 Aghakhani, S., Grandjean, D., Baekelant, W., Coutiño-Gonzales, E., Fron, E., Kvashnina K.,
383 Roeffaers M. B. J., Hofkens, J., Sels, B. F., Lievens, P. (2018) Atomic scale reversible opto-
384 structural switching of few atom luminescent silver clusters confined in LTA zeolites.
385 *Nanoscale*, 10, 11467-11476.

386 Alberti, A., Martucci, A., Galli, E., Vezzalini, G. (1997) A re-examination of the crystal structure of
387 erionite. *Zeolites*, 19, 349-352.

388 Albuquerque, R. Q., Calzaferri, G. (2007) Proton activity inside the channels of zeolite L.
389 *Chemistry, a European Journal*, 13, 8939-8952.

390 Amooghin, A. B., Omidkhah, M., Sanaeepur, H., Kargari, A. (2016) Preparation and
391 characterization of Ag⁺ ionexchanged zeolite-Matrimid® 5218 mixed matrix membrane for
392 CO₂/CH₄ separation. *Journal of Energy Chemistry*, 25, 450-462.

- 393 Arletti, R., Vezzalini, G., Quartieri, S., Cámara, F., Alvaro, M. (2013) A new framework topology in
394 the dehydrated form of zeolite levyne. *American Mineralogist*, 98, 2063-2074.
- 395 Babel, S., Kurniawan, T. A. (2003) Low-cost adsorbents for heavy metals uptake from contaminated
396 water: a review. *Journal of Hazardous Material*, 97, 219-243.
- 397 Bennett, J. M., Grose, R. W. (1978) Characterization of the offretite-levynite intergrowth from
398 Beech Creek, Oregon, by adsorption and electron diffraction. In: Sand L. B., Mumpton, F.
399 A., (eds) *Natural Zeolites*. Pergamon, Oxford, pp 77-84.
- 400 Bish, D. L; Ming, D. W. *Natural zeolites: occurrences, properties and applications*. Reviews in
401 Mineralogy and Geochemistry, 45. Mineralogical Society of America and Geochemical
402 Society, Washington DC, 2001.
- 403 Borai, E. H., Harjula, R., Malinen, R., Paaanen, A. (2009) Efficient removal of cesium from low-
404 level radioactive liquid waste using natural and impregnated zeolites minerals. *Journal of*
405 *Hazardous Material*, 172, 416-422.
- 406 Bruker AXS, APEX3 v2019.1-0.
- 407 Calligaris, M., Nardin, G., Randaccio, L. (1983) Cation site location in hydrated chabazites. Crystal
408 structure of potassium- and silver-exchanged chabazites. *Zeolites*, 3, 205-208.
- 409 Cametti, G. (2018) New topology of levyne B under quasi-equilibrium conditions: A temperature-
410 dependent in situ single crystal X-ray diffraction study. *Microporous and Mesoporous*
411 *Materials*, 265, 162-171.
- 412 Cametti, G., Scheinost, A. C., Churakov, S. V. (2019b) Structural modifications and thermal
413 stability of Cd²⁺-exchanged stellerite, a zeolite with STI framework type. *Journal of Physical*
414 *Chemistry C*, 123, 25236-25245.

- 415 Cametti, G., Scheinost, A. C., Giordani, M., Churakov, S. V. (2019a) Framework modifications and
416 dehydration path of a Ag⁺-modified zeolite with STI framework type. Journal of Physical
417 Chemistry C, 123, 13651-13663.
- 418 Colella, C. Environmental applications of natural zeolitic materials based on their ion-exchange
419 properties, in: P. Misaelides, F. Macasek, T. J. Pinnavaia, C. Colella (Eds.), *Application of*
420 *natural microporous materials in environmental technology*, Kluwer, NATO Science Series
421 vol. E362 (Applied Sciences), Dordrecht, 1999.
- 422 Coutino-Gonzales, E., Baekelant, W., Grandjean, D., Roeffaers, M. B. J., Fron, E., Aghakhani, M.
423 S., Bovet, N., Van der Auweraer, M., Lievens, P., Vosch, T. et al. (2015) Thermally
424 activated LTA(Li)-Ag zeolites with water-responsive photoluminescence properties. Journal
425 of Material Chemistry C, 3, 11857-11867.
- 426 CP2K developers group. <http://www.cp2k.org>, 2000-2019.
- 427 CrysAlisPro, Rigaku Oxford diffraction, 2018, Version 171.40.29a.
- 428 De Cremer, G., Coutino-Gonzales, E., Roeffaers, M. B. J., Moens, B., Ollevier, J., Van der
429 Auweraer, M., Schoonheydt, R., Jacobs, P. A., De Schryver, F. C., Hofkens, J., De Vos, D.
430 E., Sels, B. F., Vosch, T. (2009) Characterization of fluorescence in heat-treated silver-
431 exchanged zeolites. Journal of American Chemical Society, 131, 3049-3056.
- 432 Ferreira, L., Fonseca, A. M., Botelho, G., Aguiar, C. A., Necs, I. C. (2012) Antimicrobial activity
433 of faujasite zeolites doped with silver. Microporous and Mesoporous Materials, 160, 126-
434 132.
- 435 Flanigen, E. M., Lok, B. M., Patton, R. L., Wilson, S. T. (1986) Aluminophosphate molecular sieves
436 and the periodic table. Pure and Applied Chemistry, 58, 1351-1358.

- 437 Fois, E., Tabacchi, G. (2019) Water in zeolite L and its MOF mimic. *Zeitschrift für Kristallographie*
438 - Crystalline Materials, 234, 2018-2153.
- 439 Fron, E., Aghakhani, S., Baekelant, W., Grandjean, D., Coutino-Gonzales, E., Van der Auweraer,
440 M., Roeffaers, M. B. J., Lievens, P., Hofkens, J. (2019) Structural and photophysical
441 characterization of Ag clusters in LTA zeolites. *Journal of Physical Chemistry C*, 123,
442 10630-10638.
- 443 Gatta, G. D., Lotti, P., Tabacchi, G. (2018) The effect of pressure on open-framework silicates:
444 elastic behaviour and crystal-fluid interaction. *Physics and Chemistry of Minerals*, 45, 115-
445 138.
- 446 Gottardi, G.; Galli, E. *Natural zeolites*; Springer-Verlag Berlin Heidelberg, New York Tokyo, 1985.
- 447 Grimme, S. (2006) Semiempirical GGA-Type Density Functional Constructed with a Long-Range
448 Dispersion Correction. *Journal of Computational Chemistry*, 27, 1787-1798.
- 449 Hutson, N. D., Reisner, B. A., Yang, R. T., Toby, B. H. (2000) Silver ion-exchanged zeolites Y, X,
450 and low-silica X: Observations of thermally induced cation/cluster migration and the
451 resulting effects on the equilibrium adsorption of Nitrogen. *Chemistry of Materials*, 12,
452 3020-3031.
- 453 Inglezakis, V. J., Loizidou, M. M., Grigoropoulou, H. P. (2004) Ion exchange studies on natural and
454 modified zeolites and the concept of exchange site accessibility. *Journal of Colloid and*
455 *Interface Science*, 275, 570-576.
- 456 Kasture, M. W., Joshi, P. N., Sorti, H. S., Joshi, V. V., Choudhari, A. L., Shiralkar, V. P. (1998)
457 Sorption properties of the natural, K and partially deammoniated (H/NH₄) forms of
458 clinoptilolite. *Adsorption Science and Technology*, 16, 135-151.

- 459 Kanazawa, T. (2004) Development of hydrocarbon adsorbents, oxygen storage materials for three-
460 way catalysts and NO_x storage-reduction catalyst. *Catalysis Today*, 96, 171-177.
- 461 Knaebel, K. S., Kandybin, A. (1993) Pressure swing adsorption system to purify oxygen. US patent
462 5,226,933.
- 463 Liang, J., Zhang, R., Zhao, Q., Dong, J., Wang, B., Li, J. (2012) Molecular simulation of hydrogen
464 storage in ion-exchanged mazzite and levyne zeolites. *Computational and Theoretical*
465 *Chemistry*, 980, 1-6.
- 466 Loewenstein, W. (1954) The distribution of aluminum in the tetrahedra of silicates and aluminates.
467 *American Mineralogist*, 39, Nr. 1/2, S. 92.
- 468 Lock, B. M., Messina, C. A., Patton, R. L., Gjek, R. T., Cannan, T. R., Flanigen, E. M. (1984) U.S.
469 Patent 4,440,871.
- 470 Ma, Z., Zhang, Q., Weng, X., Mang, C., Si, L., Guan, Z., Cheng, L. (2018) Fluoride ion adsorption
471 from wastewater using magnesium(II), aluminum(III) and titanium(IV) modified natural
472 zeolite: kinetics, thermodynamics, and mechanistic aspects of adsorption. *Journal Water*
473 *Reuse and Desalination*, 8, 479-489.
- 474 Merlino, S., Galli, E., Alberti, A. (1975) The crystal structure of levyne. *Tschermaks*
475 *Mineralogische und Petrographische Mitteilungen*, 22, 117-129.
- 476 Milenkovic, J., Hrenovic, J., Matijasevic, D., Niksic, M., Rajic, N. (2017) Bactericidal activity of
477 Cu-, Zn-, Ag-containing zeolites toward *Escherichia coli* isolates. *Environmental Science*
478 *and Pollution Research*, 24, 20273-20281.
- 479 Misaelides, P. (2011) Application of natural zeolites in environmental remediation: A short review.
480 *Microporous and Mesoporous Material*, 144, 15-18.

- 481 Momma, K., Izumi, F. (2011) VESTA 3 for three-dimensional visualization of crystal, volumetric
482 and morphology data. *Journal of Applied Crystallography*, 44, 1272-1276.
- 483 Nevenka, B. P., Calligaris, M., Nardin, G., Randaccio, L. (1981) Location of cations in metal ion-
484 exchanged Zeolites. Part 2. Crystal structures of a fully silver-exchanged heulandite. *Journal*
485 *of the Chemical Society, Dalton Transactions*, 12, 2288-2291.
- 486 Ogawa, H., Ito, Y., Nakano, M., Itabashi, K. (2001) Method for adsorbing and removing ethylene
487 and method for purifying an exhaust gas. US patent 6,309,616.
- 488 Passaglia, E., Artioli, G., Gualtieri, A. (1998) Crystal chemistry of the zeolites erionite and offretite.
489 *American Mineralogist*, 83, 577-589.
- 490 Passaglia, E., Galli, E., Rinaldi, R. (1974) Levynes and erionites from Sardinia. *Contributions to*
491 *Mineralogy and Petrology*, 43, 253-259.
- 492 Passaglia, E., Sheppard, R. A. (2001) The crystal chemistry of zeolites. In: D. L. Bish and D. W.
493 Ming, Eds., *Natural Zeolites: Occurrence, Properties, Applications*, vol. 45, p. 70-116.
494 *Reviews in Mineralogy and Geochemistry*, Mineralogical Society of America, Chantilly,
495 Virginia.
- 496 Perdew, J. P., Burke, K., Ernzerhof, M. (1996) Generalized gradient approximation made simple.
497 *Physical Reviews Letters*, 77, 3865-3868.
- 498 Sacerdoti, M. (1996) New refinements of the crystal structure of levyne using twinned crystals.
499 *Neues Jahrbuch für Mineralogie Monatshefte*, 3, 114-124.
- 500 Seifert, R., Rytz, R., Calzaferri, G. (2000) Colors of Ag⁺-Exchanged Zeolite A. *Journal of Physical*
501 *Chemistry A*, 104,7473-7483.
- 502 Sheldrick, G. M. (2008) A short history of SHELX. *Acta Crystallographica A*, 64, 112-122.

503 Sheldrick, G. M., Crystal structure refinement with SHELXL (2015) *Acta Crystallographica C*, 71,
504 3-8.

505 Shimazu, M., Mizota, T. (1972) Levyne and erionite from Chojabaru, Iki island, Nagasaki Pref.,
506 Japan. *The Journal of Japanese Association of Mineralogists, Petrologists and Economic*
507 *Geologists*, 67, 418-424.

508 VandeVondele, J., Hutter, J. (2007) Gaussian basis sets for accurate calculations on molecular
509 systems in gas and condensed phases. *Journal of Chemical Physics*, 127, 114105.

510 VandeVondele, J., Krack, M., Mohamed, F., Parrinello, M., Chassaing, T., Hutter, J. (2005)a
511 Quickstep: Fast and accurate density functional calculations using a mixed Gaussian and
512 plane waves approach. *Computer Physics Communications*, 167, 103-128.

513 VandeVondele, J., Mohamed, F., Krack, M., Hutter, J., Sprik, M., Parrinello, M. (2005)b. The
514 influence of temperature and density functional models in ab initio molecular dynamics
515 simulation of liquid water. *Journal of Chemical Physics* 122: 014515.

516 Velazquez-Peña, G. C., Solache-Ríos, M., Olguin, M. T., Fall, C. (2019) As(V) sorption by different
517 natural zeolite frameworks modified with Fe, Zr and FeZr. *Microporous and Mesoporous*
518 *Materials*, 273, 133-141

519 Wang, S., Peng, Y. (2010) Natural zeolites as effective adsorbents in water and wastewater
520 treatment. *Chemical Engineering Journal*, 156, 11-24.

521 Wise, S. W., Tschernich, R., W. (1976) The chemical composition and origin of the zeolites
522 offretite, erionite and levyne. *American Mineralogist*, 61, 853-863.

523 Yamamoto, K., Ikeda, T., Onodera, M., Muramatsu, A., Mizukami, F., Wang, Y., Gies, H. (2010)

524 Synthesis and structure analysis of RUB-50, an LEV-type aluminosilicate zeolite.

525 Microporous and Mesoporous Materials, 128, 150-157.

526 Zhu, G. S., Xiao, F. S., Qiu, S. L., Hun, P. C., Xu, R. R., Ma, S. J., Terasaki, O. (1997) Synthesis

527 and characterization of a new microporous aluminophosphate with levyne structure in

528 presence of HF. Microporous and Mesoporous Materials, 11, 269-273.

529 Zukal, A., Pulido, A., Gil, B., Nachtigall, P., Bludský, O., Rubeš, M., Čejka, J. (2010) Experimental

530 and theoretical determination of adsorption heats of CO₂ over alkali metal exchanged

531 ferrierites with different Si/Al ratio. Physical Chemistry Chemical Physics 12, 6413-6422.

532

533

534

535

536

537

538

539

540

541

542

543

544

545

546

547

548 **Table 1** Relevant bond distances (Å) of Ag-levyne structure at room temperature.

Framework			
T1-O4	1.6431(14)	T2-O5 ×2	1.6391(12)
T1-O1	1.645(3)	T2-O1 ×2	1.647(3)
T1-O3	1.6558(16)	<T2-O>	1.643
T1-O2	1.6800(19)		
<T1-O>	1.656		
Extraframework			
Ag1-W1	×3 2.372(8)	Ag4A-O1	×2 2.684(13)
-O2	×3 2.470(5)	-W3	×2 2.77(3)
		-O5	×2 2.765(11)
Ag2-O5	×6 2.591(5)		
Ag2A-O5	×3 2.682(7)		
Ag2B-W3	×3 2.60(3)		
Ag3-W1	×3 2.33(2)		
-W3	×3 2.34(3)		

549

550 **Table 2** Unit-cell parameters of Ag-levyne obtained from MD trajectories and SC-XRD data

551 collected at RT. The deviation (in percentage) of MD unit-cell parameters from those obtained by

552 SC-XRD is shown.

	MD	XRD	Deviation
<i>a</i> -axis (Å)	13.47(8)	13.4169(3)	0.43%
<i>b</i> -axis (Å)	13.52(8)	13.4169(3)	0.79%
<i>c</i> -axis (Å)	22.98(14)	22.5926(6)	1.75%

553	α (°)	90.16	90	0.17%
	β (°)	89.90	90	0.11%
554	γ (°)	119.99	120	0.009%
	Cell volume (Å ³)	3621(13)	3522.09(18)	2%

555

556

557 **Table 3** Relevant bond distances (Å) of Ag-erionite structure at room temperature.

558

Framework				
559	T1-O1	1.651(2)	T2-O3	1.6231(18)
	T1-O2	1.634(2)	T2-O4 ×2	1.649(4)
560	T1-O4	1.649(4)	T2-O5	1.646(3)
	T1-O6	1.650(2)	<T2-O>	1.642
561	<T1-O>	1.646		

562

Extraframework					
563	K1-O1	×6	2.941(6)	C3-W4A ×2	2.63(2)
	K1A-O1	×3	2.51(11)		
564	K1A-O6	×3	3.09(17)		
565	C1-O6	×2	2.500(6)		
	-O4	×2	2.986(5)		
566	C2-O5	×3	2.487(11)		
567	C2A-O5	×3	2.410(10)		
	C2B-O5	×3	2.640(14)		
568	-W5		2.29(6)		

569

570

571

572

573

574

575

576

577

578 **Figure Captions**

579

580 **Figure 1** SEM BSD images of levyne-erionite intergrowths.

581

582 **Figure 2** Crystal structure of Ag-levyne projected along [110]. Blue spheres represent the (Si,Al)
583 tetrahedral sites, silver and oxygen atoms are displayed in grey and red, respectively. Partially
584 colored spheres correspond to partial occupancy of the crystallographic sites. The yellow line
585 indicates the three-fold axis.

586

587 **Figure 3** A snapshot of Ag-levyne structure after 18 ps MD simulation. Color code as in Figure
588 2. Al-occupied tetrahedral sites are shown as dark cyan spheres. Ag-O bonds are shown with
589 grey lines.

590

591 **Figure 4** Radial distribution function (RDF) (continuous line) and coordination number (CN)
592 (dotted lines) of Ag-O and Ag-Ow distances of Ag-levyne calculated from MD trajectories.

593

594 **Figure 5** Silver and water molecules distribution within the *lev* cavity of the (a) calculated
595 (snapshot after 18 ps calculation) and refined (b) Ag-levyne structure.

596

597 **Figure 6** Crystal structure of Ag-erionite refined from XRD. Color code as in Figure 2. Purple
598 spheres represent K atoms. Grey lines indicate Ag-O bonds in the *eri* cavity.

599
600 **Figure 7** Perspective view of the simulated (11 ps) Ag-levyne supercell with 2 H₂O per Ag ions.
601 Color code as in Figure 3. Ag ions are not found in the D6R cages.

Figure 1

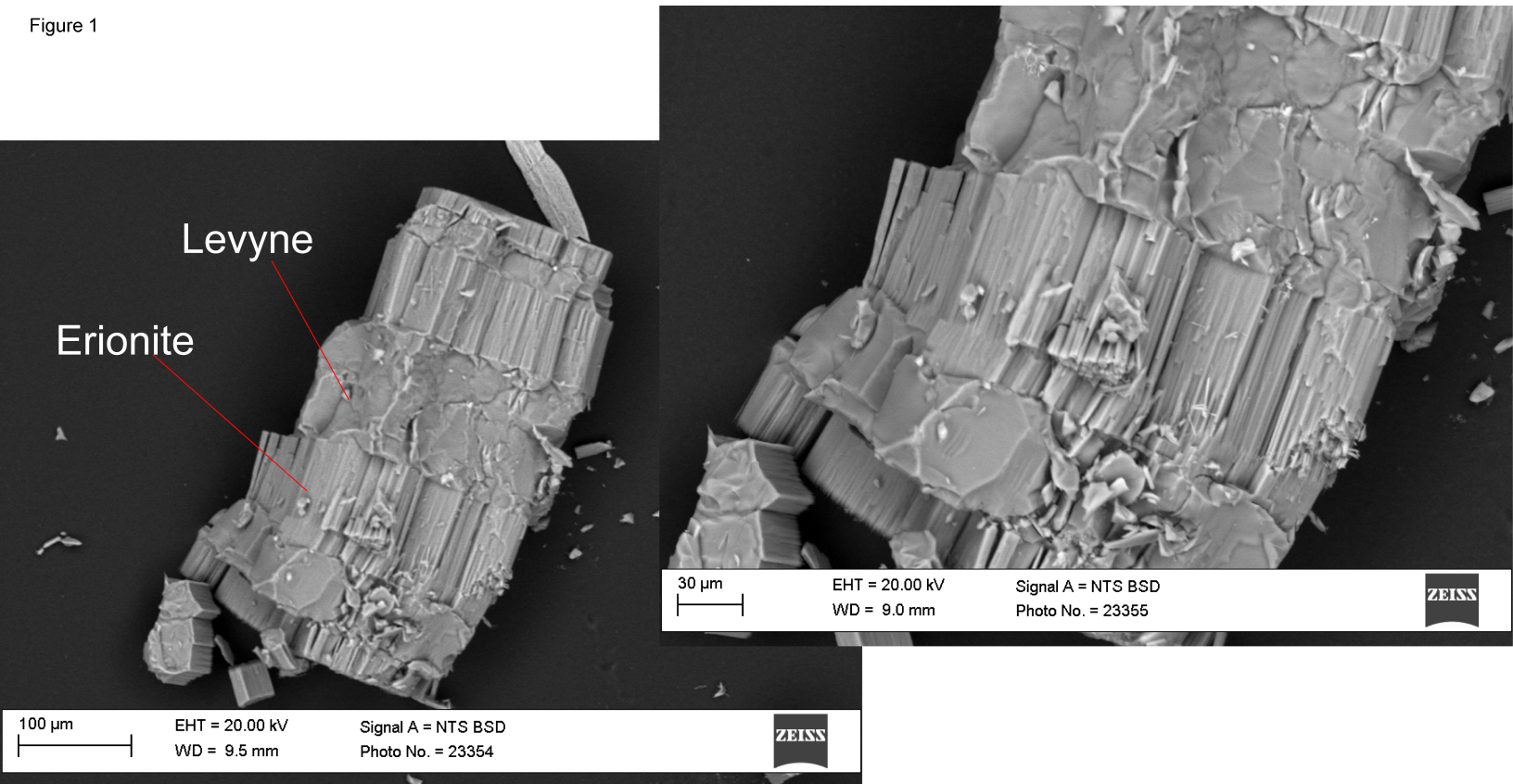


Figure 2

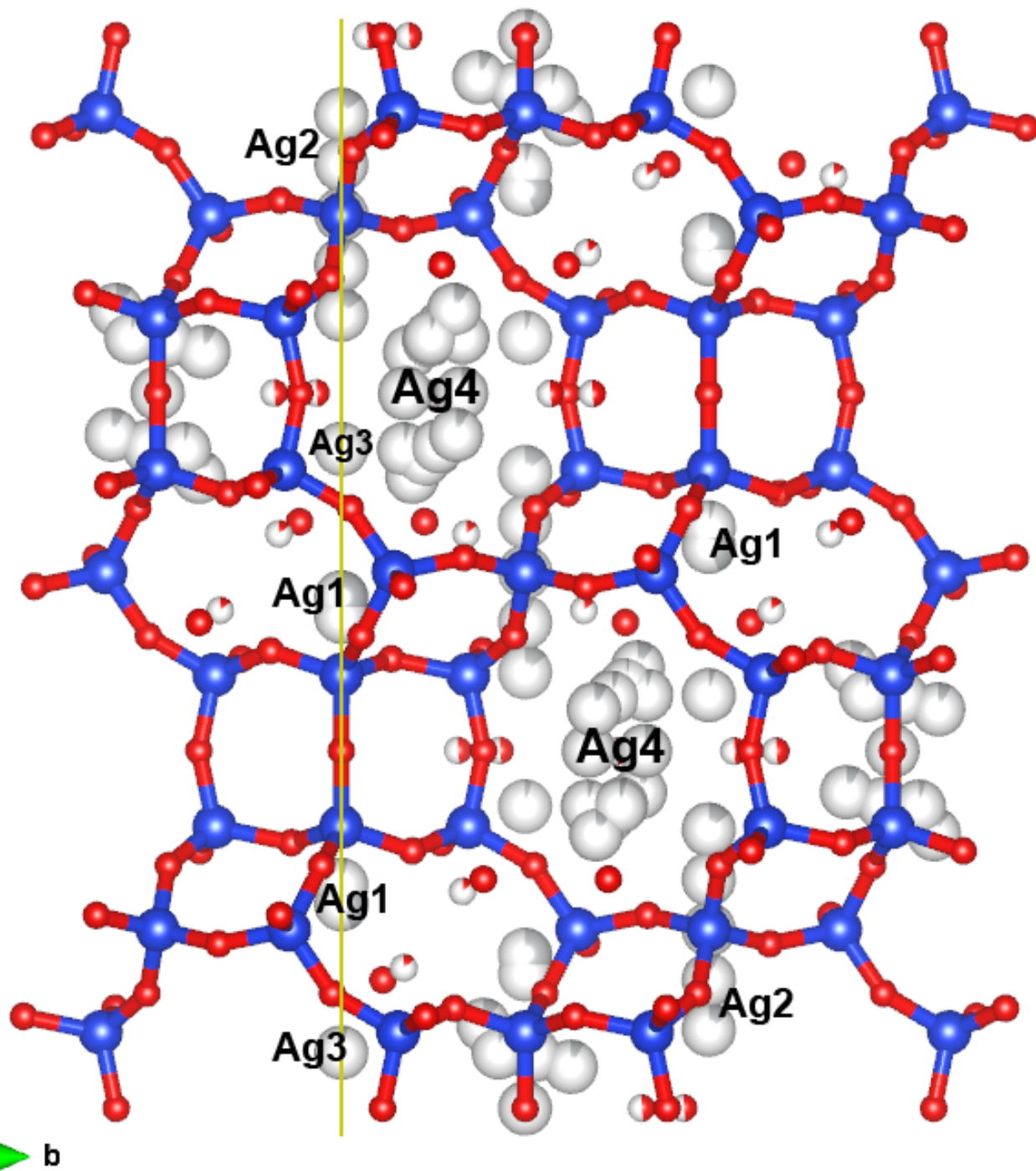


Figure 3

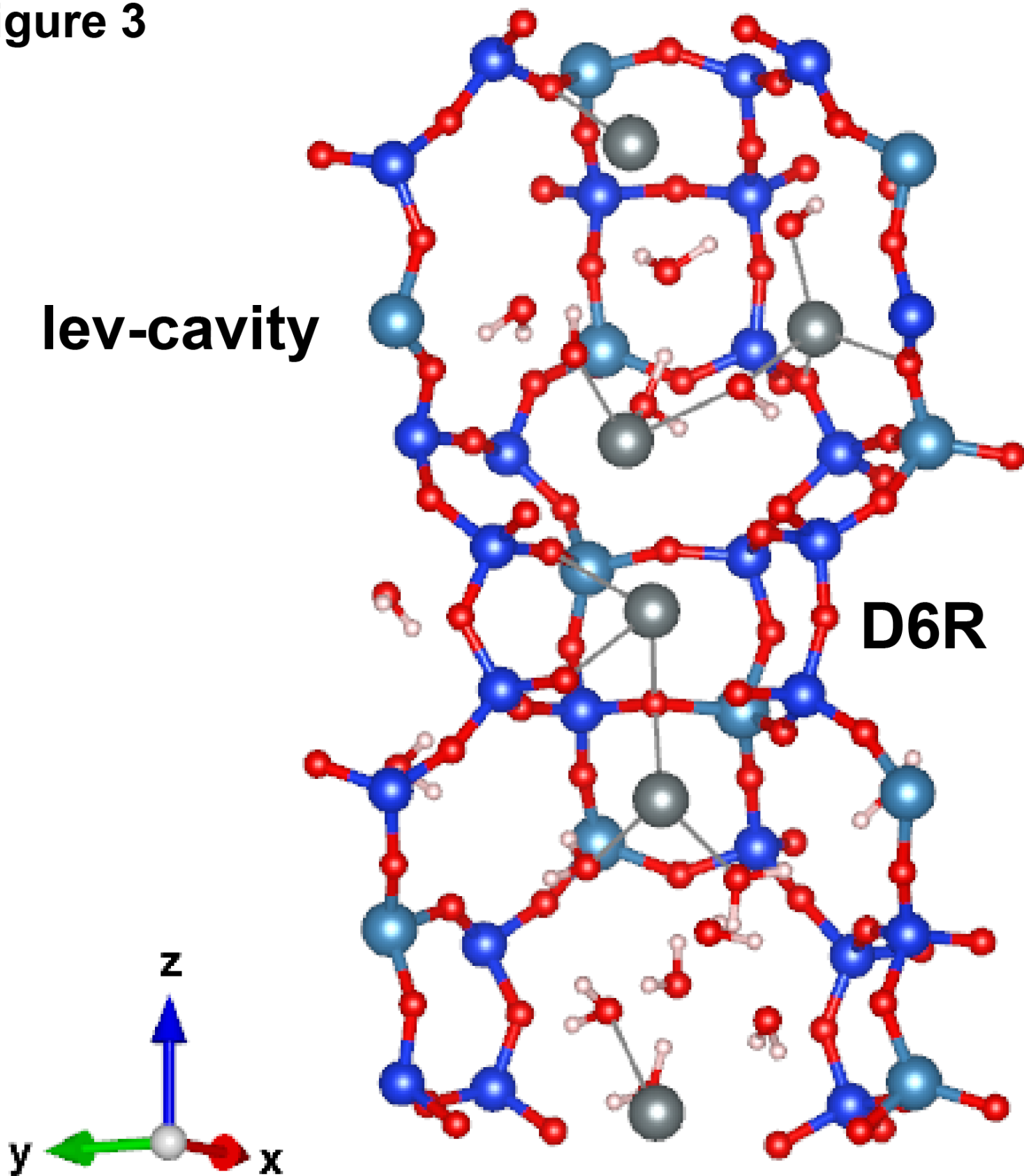


Figure 4

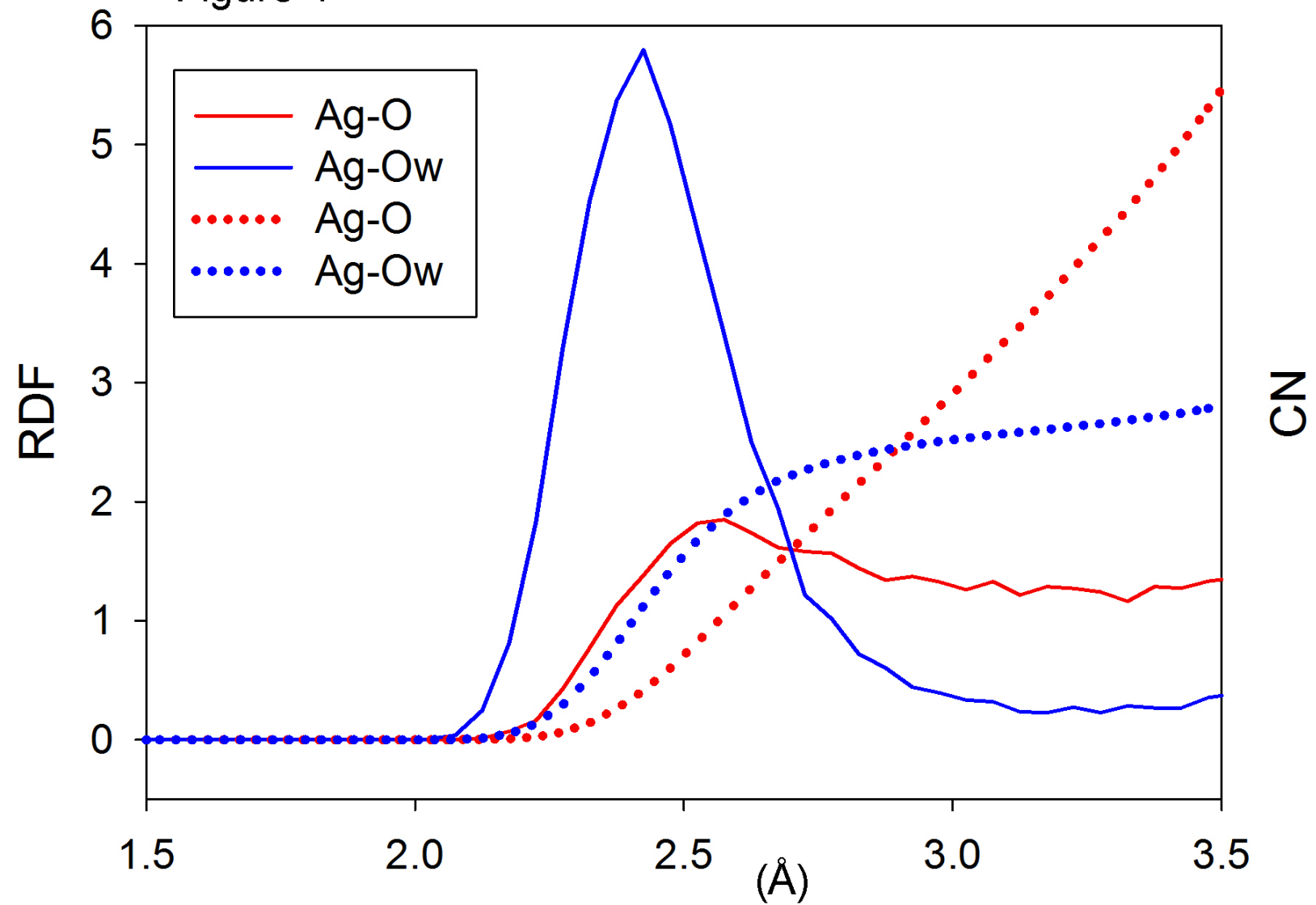
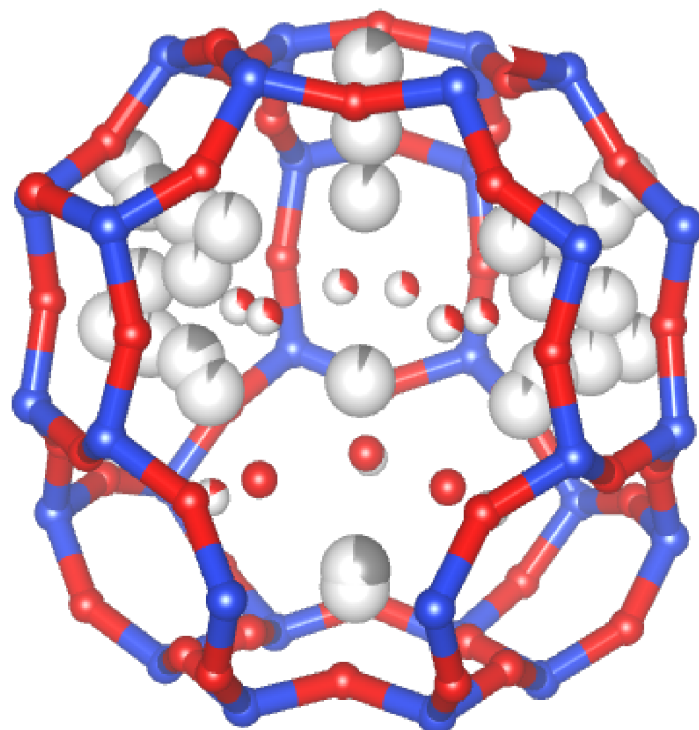
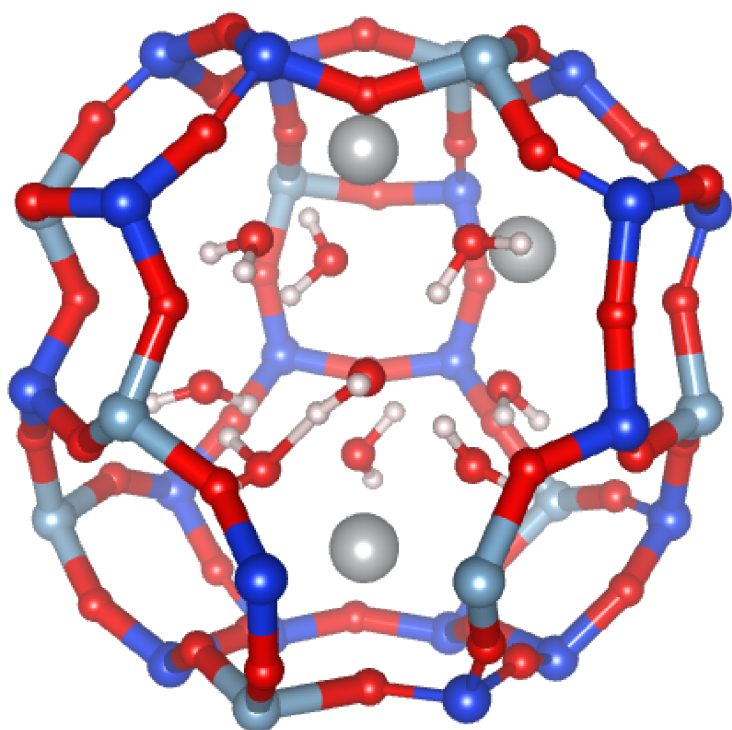


Figure 5

MD

XRD



lev-cavity

a

b

Figure 6

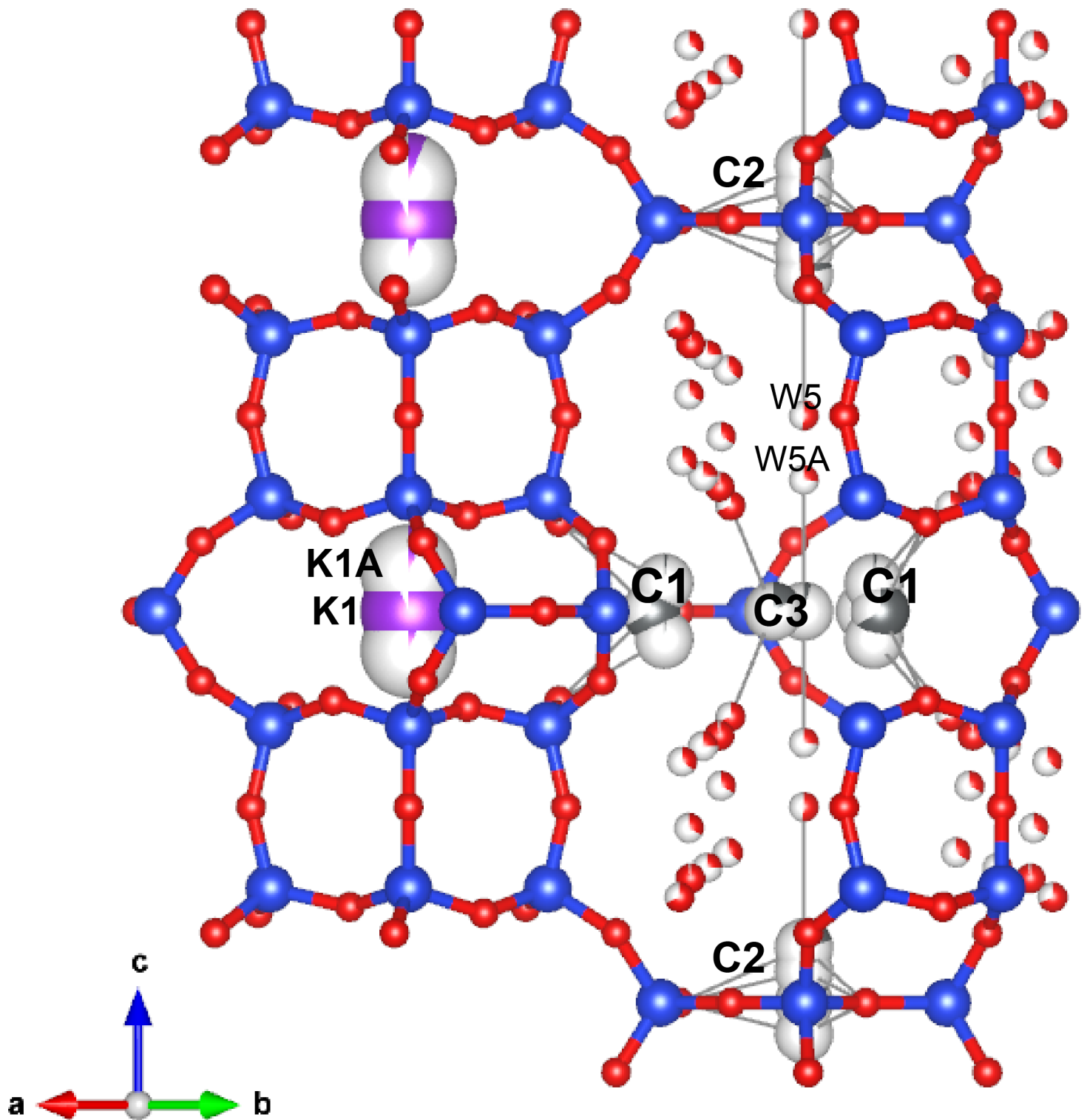


Figure 7

